WAVELET-BASED NOISE REMOVAL FROM RAMAN SIGNAL TO STUDY PLD COATED FORSTERITE-HYDROXYAPATITE THIN FILM ON STAINLESS STEEL 316L SUBSTRATE[**]

P. S. Prakash [1], T. S. Sharan [2], S. J. Pawar [1], R. P. Tewari [1*], S. Sharma [2]

[1] Department of Applied Mechanics, Motilal Nehru National Institute of Technology Allahabad, Prayagraj-211004, Uttar Pradesh, India; e-mail: pspsbme@gmail.com; tareshss.rs.bme16@itbhu.ac.in; sjpawar@mnnit.ac.in; rptewari@mnnit.ac.in; shiru.bme@iitbhu.ac.in
[2] School of Biomedical Engineering, Indian Institute of Technology (BHU), Varanasi-221003, Uttar Pradesh, India

Raman spectroscopy is proposed here for the study of forsterite-hydroxyapatite (FS-HA) composite coating on a stainless-steel substrate. However, in order to analyze the Raman spectrum accurately, noise and background removal is always required. A comparative study has been done for the correction of background. The wavelet-based denoising of the signal was done using level 6 decomposition with sym4 wavelet and the thresholding method used was soft thresholding. In the present work, the effectiveness of the wavelet-based denoising method has been compared with Savitsky–Golay smoothing, quadratic regression, and low pass filter method. It is found that the wavelet-based denoising method works better as compared to other methods as it is able to smooth the signal and to increase the SNR while maintaining the peak intensity undistorted. Peaks are calculated for the different composition of the HA-FS composite. The variation of peak location in the processed Raman spectra suggests that the variation in concentration of FS and HA in the coating can be studied by using Raman spectroscopy.

Keywords: *Raman spectroscopy, MATLAB, Pulse Laser Deposition, signal processing, Forsterite, stainless-steel.*

УДАЛЕНИЕ ШУМА НА ОСНОВЕ ВЕЙВЛЕТ-МЕТОДА ИЗ СПЕКТРА КОМБИНАЦИОННОГО РАССЕЯНИЯ ДЛЯ ИССЛЕДОВАНИЯ ТОНКОЙ ПЛЕНКИ ФОРСТЕРИТ-ГИДРОКСИАПАТИТА, ПОЛУЧЕННОЙ ИМПУЛЬСНЫМ ЛАЗЕРНЫМ ОСАЖДЕНИЕМ НА ПОДЛОЖКЕ ИЗ НЕРЖАВЕЮЩЕЙ СТАЛИ 316L

P. S. Prakash [1], T. S. Sharan [2], S. J. Pawar [1], R. P. Tewari [1*], S. Sharma [2]

УДК 535.375.5;539.216.2

[1] Национальный институт технологий Motilal Nehru, Аллахабад, 211004, Уттар-Прадеш, Индия; e-mail: pspsbme@gmail.com; tareshss.rs.bme16@itbhu.ac.in; sjpawar@mnnit.ac.in; rptewari@mnnit.ac.in; shiru.bme@iitbhu.ac.in
[2] Школа биомедицинской инженерии, Индийский технологический институт (BHU), 221003, Варанаси, Уттар-Прадеш, Индия

(Поступила 21 мая 2019)

Для исследования форстерит-гидроксиапатитного композитного покрытия на подложке из нержавеющей стали предлагается использовать КР-спектроскопию. Однако для выделения спектра КР требуется удаление шума и фона. Для коррекции фона применен метод сравнения. Основанное на вейвлет-подходе шумоподавление сигнала выполнено с помощью шестого уровня декомпозиции с вейвлетом sym4 при мягком преодолении порога. Проведено сравнение эффективности вейвлет-метода шумоподавления с методами сглаживания Савицкого–Голея, квадратичной регрессии и

[**] Full text is published in JAS V. 87, No. 3 (http://springer.com/journal/10812) and in electronic version of ZhPS V. 87, No. 3 (http://www.elibrary.ru/title_about.asp?id=7318; sales@elibrary.ru).

фильтрации низких частот. Установлено, что метод вейвлет-шумоподавления работает лучше, чем другие методы, так как способен сглаживать сигнал и увеличивать отношение сигнал/шум, сохраняя пиковую интенсивность неискаженной. Пики рассчитаны для различных составов форстерит-гидроксиапатитного композита. Изменение расположения пиков в обработанных спектрах КР позволяет предположить, что изменение концентрации форстерита и гидроксиапатита в покрытии может быть исследовано с помощью спектроскопии КР.

Ключевые слова: *КР-спектроскопия, MATLAB, импульсное лазерное напыление, обработка сигналов, форстерит, нержавеющая сталь.*

Introduction. Forsterite (FS) is a mineral that belongs to the olivine group and commonly found in the upper mantle layer of the earth's crust [1]. It has an orthorhombic crystal structure with the chemical formula Mg_2SiO_4 and is named after the German naturalist Johann Forster. FS has shown superior biological and mechanical properties desirable for coating material on implants [2, 3]. However, presently it is not extensively explored as a coating material for metallic implants. Hence, FS has been selected for this study, which focuses on exploring its potential application as a coating material on metallic implants.

Recently, hydroxyapatite (HA) is one of the most commonly used material for coating on implants due to its chemical composition (chemical formula $Ca_{10}(PO_4)_6(OH)_2$), which is similar to natural bone. Moreover, HA can be easily synthesized in powder form, which is suitable for coating applications. Levitt et al. started the application of HA in medical science in 1969. They hot-pressed the HA powder and molded it into different useful shapes for their biological experimentation [4]. This initial research unfolded the biomedical applications of HA mineral, and numerous research papers have appeared focusing on the various aspects of HA as bone cement, composites, etc. [5–7].

Various types of biomaterials such as metals [8, 9], polymers [10, 11], ceramics [12], and composites [13] have always attracted the interest of clinicians and researchers in the functional development of various part of the human body. The biological system of the human body has a fundamental nature: it always rejects foreign materials/invasion. So, it is always a key concern to check biofunctionality and biocompatibility before the use of such materials. Generally, the corrosion problem still persists in the case of using metals and alloys. Many approaches have been explored by various researchers to improve various properties of metals and their alloys. One common and easy method that has been developed is a biocompatible coating over medical implant [14–18].

The Raman effect was discovered in 1929, but it remained on the theoretical level due to low sensitivity and overlapping fluorescence phenomena. However, the use of Raman spectroscopy in the characterization of material increased remarkably in the last three decades due to advancements in available detectors and filters for the Raman system. The composition of materials influences the physical properties of the product and thus the characteristic of the material. Raman spectroscopy is a powerful optical tool that helps in the identification of materials and gives information on the structure without the destruction of the sample. Every material has its own unique Raman fingerprint, which can be used to identify the presence in the composition of materials. Raman molecular spectroscopy is suitable for qualitative analysis. However, it can also be used for quantitative study as the intensity of Raman scattered light is proportional to the amount of material present in the sample.

In this work, the combination of FS-HA as the composite coating has been used over medical grade alloy i.e., stainless steel (SS 316L), using the pulse laser deposition (PLD) technique. The main focus of this study is to validate the presence of forsterite and hydroxyapatite using Raman spectroscopy in the coating film as their ratio in the coating materials is varied as given in Table 1. Signal preprocessing techniques are applied to remove fluorescence background, and background removal is done along with smoothing to find the dominant peaks in the signal effectively. To our best knowledge, no Raman analysis of FS-HA thin-film coating is done to date. It is a very new approach to evaluate the thin film in this way because sometimes it becomes hard to know the chemical compositions of the thin film having a thickness approximately in the nanometer regime.

Materials and experimental methods. *Synthesis of forsterite.* Synthesis of forsterite (FS) powder was done using the sol-gel method, which is explored by Prakash et al. [19]. The precursors such as magnesium nitrate hexahydrate and sucrose were procured from Merck, Germany. Polyvinyl alcohol (PVA), nitric acid, and Ludox SM colloidal silica (30 wt.% suspension in H_2O) were procured from Sigma-Aldrich, USA.

The hydroxyapatite (HA) powder, according to the standards given in Khandelwal et al. [20], was commercially available, and it was procured from Clarion Pharmaceutical Co., New Delhi, India.

Preparation of PLD targets. Both the powder FS and HA were gently mixed together with 1% of PVA soluti on using a mortar-pestle. For making PLD targets, the FS/HA was taken as in parts ratio and is listed in Table 1.

TABLE 1. The Different Composition Used for Coating on a Stainless Steel Target

Material	P1[#]	P2[#]	P3[#]	P4[#]	P5[#]
FS powder (in part)	–	1	2	3	10
HA powder (in part)	10	9	8	7	–

[#]P1, P2, P3, P4, and P5 are Pallets (Targets).

Targets of the required size (diameter ~25 mm) and thickness (~4 mm) were fabricated by compressing the mixture of FS and HA powders with the help of an Ultimate Tensile Machine (UTM). The targets were heat-treated at 1000°C for 4 hours for greater densification and further removal of other volatiles as well.

Coating using PLD technique. The laser system used in this study is a Nd:YAG (Instruments-Model: Quanta System Q1 DNA) operated at 355 nm at 8 Hz repetition rate with eight ns pulse duration. The deposition was done in a stainless-steel vacuum chamber at a maintained pressure of 10^{-5} mbar. The sintered target was kept on the target holder, 4 cm away, and exactly parallel to the substrate, which rotated for uniform laser ablation. The deposition was performed on a heated substrate at 650°C. The plasma plume can be seen inside the chamber, where it is generated by a laser beam incident on the target, by which the deposition was done on the substrates.

Raman spectra acquisition. A Raman spectrometer (Renishaw, UK) equipped with 532 and 785 nm laser source was used to acquire the Raman data from the coated substrates. Only 1% of total available power (5 mW/mm^2) of 532 nm diode-pumped solid-state laser excitation was used to avoid heating of the sample. The 50× short distance objective lens was used to focus the excitation laser on the sample. The Raman scattered light is collected back in backscattering geometry using the same objective lens, and a 2400 groove/mm grating was used as a dispersion element. The slit width was maintained at 50 μm during measurement. The resolution of the spectrometer is better than 1 cm^{-1} with a repeat deviation of fewer than ±0.2 cm^{-1}. Spectrometer scanning and data collection were done on a dedicated computer using the Wire 4.0 software. The recorded spectrum is further pre-processed to remove background and noise using MATLAB for calculation of peaks. Processed spectra were plotted using Origin 8 software.

Signal pre-processing. The obtained Raman signals are affected by the intrinsic fluorescence properties of the sample under the test. Moreover, due to the instrumental response of the apparatus, the signals are contaminated with noise. The Raman spectroscopy is a weak phenomenon and thus is affected by the noise, which will reduce the accuracy and precision of the analysis. Measurement with sensitive, stable instrumentation and in optimal conditions is recommended to reduce noise. However, it is not always possible to obtain such a situation. Hence, signal pre-processing is required to analyze the spectrum effectively.

Background removal. The application of Raman spectroscopy in the analysis encounters several challenges, among which background and noise are prominent ones. Backgrounds can be several times more intense than weak Raman signal, and hence the removal of these backgrounds is essential for accurate qualitative and quantitative analysis of the sample. Some of the research works concentrated on the removal of background and noise to extract spectral information [21] efficiently. A number of background removal methods have been previously proposed, such as wavelength shifting, frequency-domain filtering, and first- and second-order derivative. These methods show good results in the specified situation. However, these have some limitations too, while polynomial fitting has the advantage of retaining spectral features and intensities of the spectra. In this background correction method, the coefficient of polynomial $P(X)$ of degree N is required to fit the data by a least-square method. Another background removal method is spline fitting, which is one of the best background removal techniques available for spectral analysis. In present work, the background in the signal with peaks is adjusted in three steps. It starts with selecting a window of 200 samples from the start of the signal and estimating the background for the window size and then moving to the next sample group. Further, it applies regression to these windows, and the final background is estimated using a spline fitting approximation. The background was then subtracted from the input signal to remove the background.

Denoising. The intensity of Raman spectra mostly depends on laser power but is limited by the maximum power that a sample can withstand without damage. In this case, the laser has to operate at low power; however, this also introduces a high level of noise in the spectra. Further, in analysis such as peak detection,

some degree of denoising is required where raw spectra are convolved with some weighted smoothing function. The basic smoothing technique is an equally weighted moving average where each point in the smoothed spectrum Y is the average of N points from the raw spectrum S as expressed by the following expression:

$$Y[n] = \frac{1}{N}\sum_{i=0}^{N-1} S[n+i], n = 1,2,3,\ldots\ldots N\,, \quad (1)$$

where N is the number of points used in the moving average filter and n is the running index of the ordinate data.

The Savitzky-Golay smoothing is another simplified method for spectrum smoothing using the least square technique, preserving peaks and valleys of the spectrum [22, 23]. Moreover, the Savitzky-Golay smoothing proved to work satisfactorily for the Raman spectrum; however, small and split peaks are also removed in some cases. Another way for denoising the spectrum data is wavelet denoising. Here, it is assumed that the background, noise, and Raman peaks are well separated in the transformed domain as noise is considered to be a high-frequency component, the background to be a low-frequency component, and Raman signal to be a mid-frequency component [24—26]. Generally, the denoising of spectral data using the wavelet transform is carried out in three steps:

1. Decompose: the wavelet type is selected, and the signal is decomposed to level L.

2. Threshold detail coefficient: for each level detail coefficient, the threshold is selected and soft or hard thresholding is applied.

3. Reconstruct: the signal is reconstructed using the modified details coefficients of levels 1 to L and the original approximation coefficient of level L.

Initially, sym2, sym3, sym4, db1, db2, and db3 were used with 4, 5, and 6 levels of decomposition to check wavelet type. The level of decomposition was giving the optimal result. The results showed that sym4 with six levels of decomposition gives the best result among all considered combinations and is thus further used for the denoising. The "Byes method" was used to determine the threshold value for decomposition, and the median was used for threshold rule. A comparative study was also done for denoising capability with other methods such as quadratic regression, low pass filtering, and Gaussian denoising.

Performance indicator. The intensity of the characteristic peak ($I_{\max}$), the goodness of fit, and SNR are used to measure the ability of different denoising methods mentioned above. The goodness of fit compares the spectrum data X with reference spectrum X_{ref} using some measure function such as mean square error (MSE) or normalized mean square error (NRMSE) to produce fitness. It is a quantitative representation of the closeness of X to X_{ref}. In this study, the background-corrected spectrum was taken as reference data, and the denoised spectrum was compared to evaluate the data closeness. The performance indicator SNR was used for the quantitative measurement of the desired signal level to noise level, calculated as

$$\text{SNR} = I_{\max} \Big/ \sqrt{\frac{\sum_{m=0}^{N} V_s^2}{N}}\,, \quad (2)$$

where N is the number of data points in the featureless region and V_s is the denoised signal.

Peak detection. The Raman spectrum of a sample is a requisite condition to analyze the accurate position of each peak. Moreover, the Raman spectra are oftentimes overlapped with fluorescence background and high level of noise due to instrumentation limits. This makes the peak finding difficult, especially if the low intensity or split peak is there in the spectra. Due to this reason, background removal and smoothing are done first. Generally, peaks are determined by finding local maxima in the data vector. A local maximum is defined as a peak if it is either larger than two neighboring samples or is equal to infinity. Different restrictions can be applied to specify the peaks of interest. In the case of the Raman spectrum, this process becomes difficult because of inefficient determination of threshold value and peak-to-peak distance for locating maxima. In the said case, after capping the number of peaks, the range of the spectrum was selected manually to capture the peak occurrence by introducing threshold intensity and peak distance restrictions. The same procedure is repeated for the whole range of spectra. This procedure helped to determine the peak position and Raman intensity accurately.

Result and discussion. The Raman spectrum was acquired from eleven samples, including bare stainless-steel sheet, five palettes of different compositions of HA-FS, and five PLD coated HA-FS on stainless steel. Initially, the palettes were prepared for different compositions of HA-FS, and the same proportion of composite was coated to stainless steel using PLD, as described in Table 1. Raman spectrum was recorded using Wire 4.0 software and was exported as an excel file so that further processing and analysis can be carried out using MATLAB.

Background correction. The captured Raman spectrum file was imported in MATLAB and plotted to check the type of background removal required. On the basis of background, viz. offset from zero axes, initial transient, linear trend, and polynomial trend, a total of four spectra was selected. Furthermore, the background removal was carried out using a polynomial fit, spline fit, and linear detrend method. The recorded Raman spectrum with an offset from the background is shown in Fig. 1a. All of the three background removal methods worked satisfactorily for this type of background. Figure 1b shows the background; system transient caused the visualization and extraction of the peak at 410 cm^{-1} to be difficult. The initial value of the spectrum increased abruptly. The background removal method resulted in a visible peak. Figures 1c, d show the linear and polynomial background of the Raman spectrum and corrected spectrum using different methods. The linear detrend method was found unsuitable in the case of the polynomial type of background. Except for this, all spectra resulted in improved SNR and undistorted peak values pertaining to background removal. This analysis resulted in the conclusion that the spline fit background removal method is best situated under such a scenario.

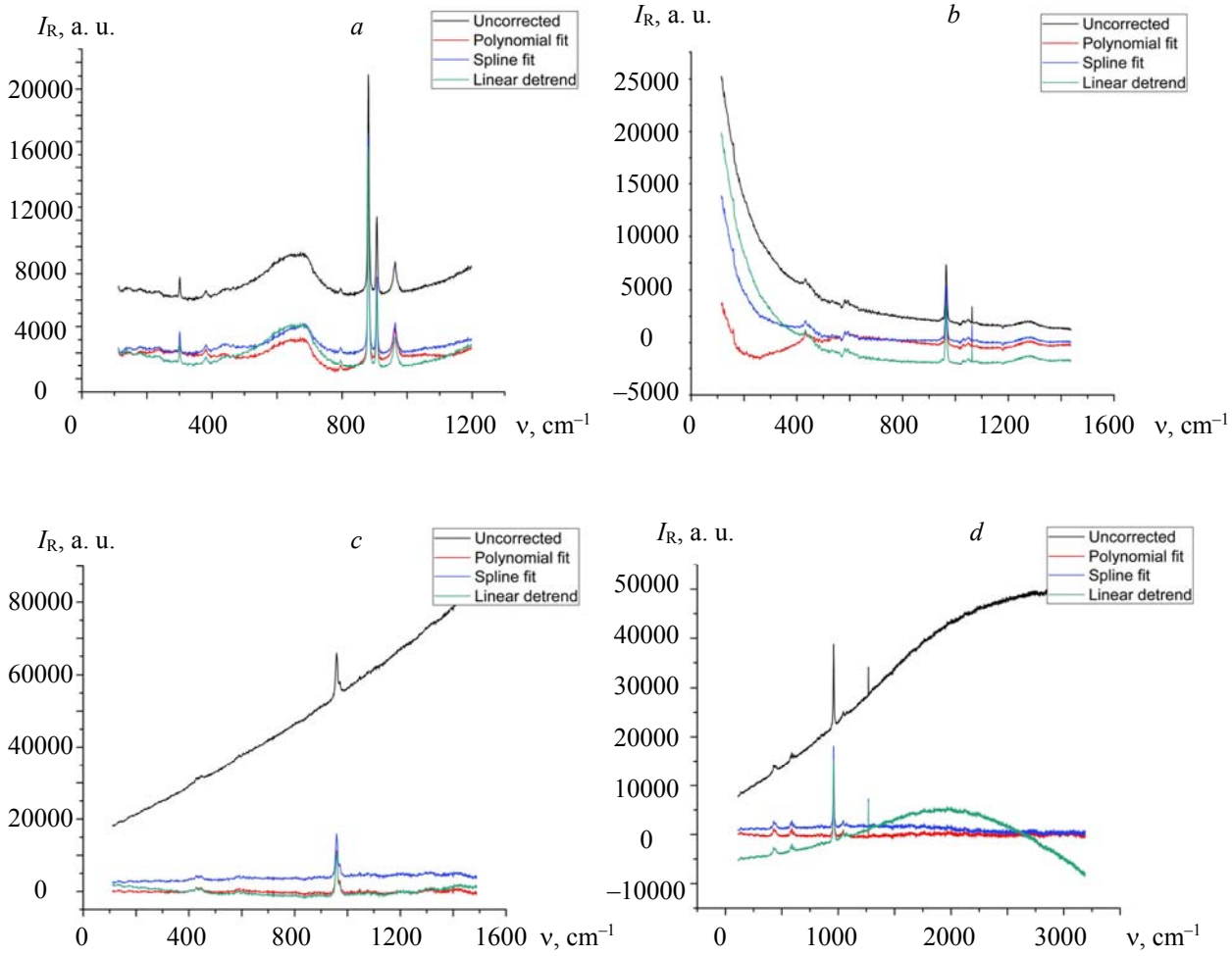

Fig. 1. Polynomial, spline, and linear detrend background removal method applied to different types of background shifts: a) offset from zero lines; b) initial transient; c) linear trend; d) polynomial trend.

Denoising. The spectral smoothing, in connection with background removal, plays a significant role in improving the SNR. The improved SNR for a signal will increase the possibility of extracting molecular fingerprints more accurately. In this study, there were four denoising methods considered, viz. Savitsky-Golay, wavelet denoising, quadratic regression, and low pass filter. Raman spectrum is considered, and denoising is applied to CP3 (coated stainless steel, sample with 20% FS and 80 % HA). Figure 2 shows the spectrum from 200 to 420 cm^{-1} only to better visualize the effect of the denoising method. The final pro-

cessed spectrum for CP1 to CP5 is shown in Fig. 3. The intensity of characteristic peak, SNR, and goodness of fit was used to measure the performance of the smoothing methods. The goodness of fit and SNR were used to select the most appropriate method for smoothing the Raman signal. The best method should improve the goodness of fit and SNR without reducing the characteristic intensity peak. The performance index of different denoising methods is shown in Table 2.

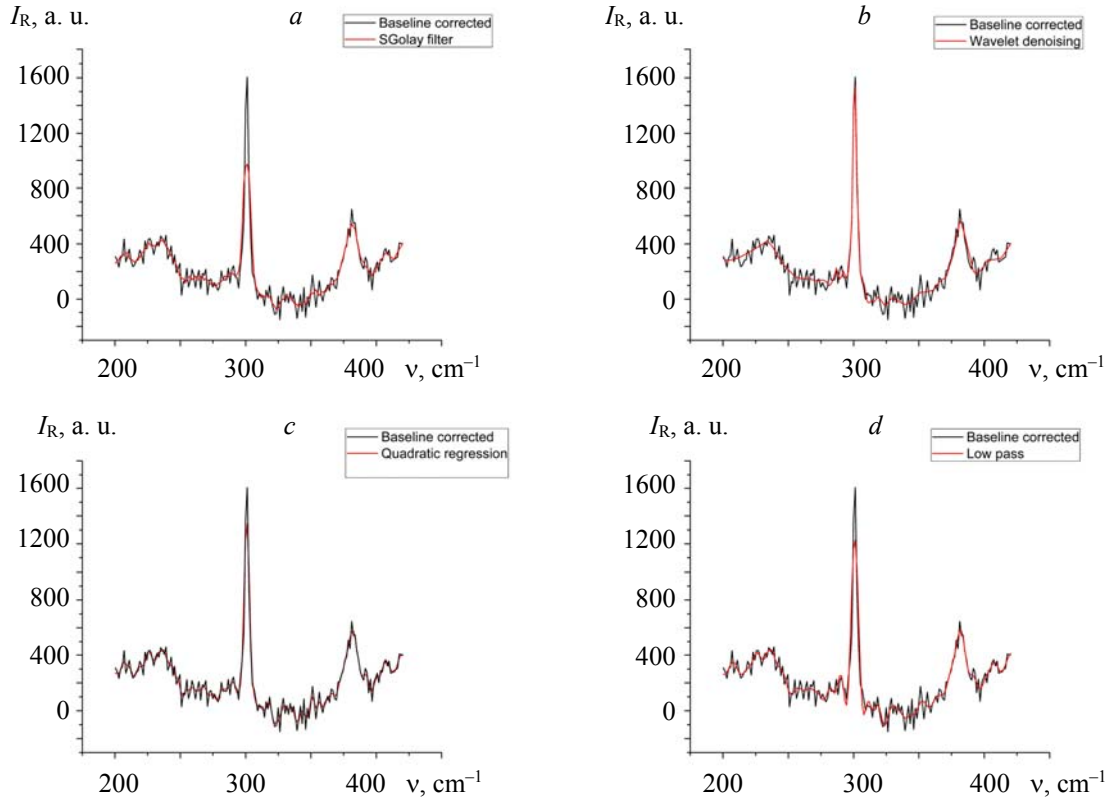

Fig. 2. Denoising method applied to background corrected spectrum: a) Savitsky-Golay filter; b) wavelet denoising; c) quadratic regression denoising; d) low pass filter denoising.

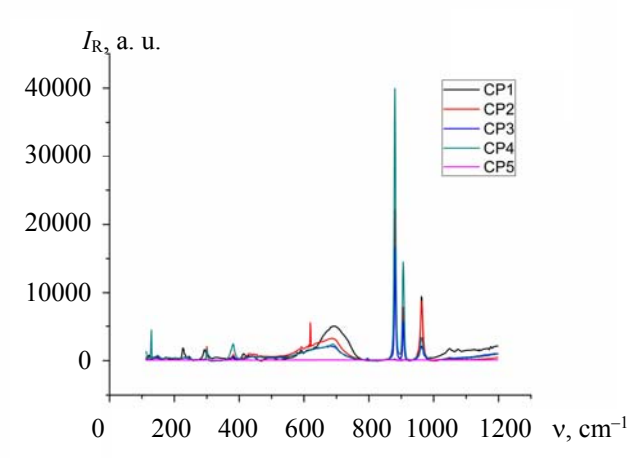

Fig. 3. Processed Raman spectrum of different coatings on stainless steel 316L: CP1 (100% HA), CP2 (90% HA, 10 % FS), CP3 (80% HA, 20% FS), CP4 (70% HA, 30% FS), CP5 (100 % FS).

For stainless steel 316L coated with 30% FS and 70% HA (CP4), the goodness of fit, SNR, and characteristic peak value after processing the spline fit background corrected spectrum were considered. The Savitsky-Golay filter gives the best SNR for the given signal. However, the intensity of the characteristic peak and

goodness of fit with respect to the background corrected spectrum were found to be much lower. On the other hand, wavelet denoising is able to maintain the characteristic peak intensity near to the non-processed spectrum with the goodness of fit of 0.944. Further, it is also able to improve the SNR of the signal, too, and this reveals that the wavelet denoising method proved better for Raman spectrum denoising.

TABLE 2. The Performance Index of Different Denoising Methods

Method	I_{max}	The goodness of fit (reference background corrected signal)	SNR
Background corrected	16613.8029	–	14.9646
SG	11819.6655	0.7288	17.7798
Wavelet	16632.1552	0.9444	16.2121
Quadratic regression	15044.9784	0.9098	16.1483
LPF	14162.7748	0.8340	16.2681

The Raman spectrum for 316L medical grade uncoated stainless-steel shows a sharp peak at 556 cm^{-1}, which is mainly due to $Fe_{2.6}Cr_{0.4}O_4$ formation on the surface [27]. Further, a broadband peak with a maximum at 716 cm^{-1} was also observed. This broadband appears due to the oxidization of the upper layer of the stainless steel. The Raman spectra of the oxidation layer were reported to be around 708 cm^{-1}. This shift may appear due to the presence of a higher degree of crystal disorder and/or strain [28]. The stainless steel is required to be protected from such an oxidizing layer so that it can be used for biomedical applications. To achieve this, the HA-FS composite with varying amounts of HA and FS was coated on the stainless steel for further improvement of biocompatibility for implant application. The major peaks and their assignment to different modes in HA are shown in Table 3.

TABLE 3. Peak assignments to different Raman peaks of Hydroxyapatite

Peak, cm^{-1}	Assignment	Reference
410	O-P-O bending modes (ν_2) of the HPO_4^{2-} group	[29]
961	Totally symmetric stretching mode (ν_1) of the tetrahedral PO_4 group (P-O bond)	[30, 31]
883, 917	P-OH stretching mode (ν_1) of the HPO_4^{2-} group	[32, 33]
1050, 1073	Triply degenerate asymmetric stretching mode (ν_3) of the PO_4 group (P-O bond)	[32, 34]

Finally, the coating was done with hydroxyapatite only (CP1), and the major peak in the Raman spectrum was found at 410, 961, 1050, and 1073 cm^{-1}. These Raman peaks are mainly due to P-O and O-P-O bond bending and stretching modes. Further, the coating was done using 90% HA and 10% FS (CP2). Additional Raman peaks at 880 and 906 cm^{-1} appear for the coatings composite of HA-FS. This confirms that the presence of FS makes the HA more Raman active. The peaks at 880 and 906 cm^{-1} are due to the P-OH bond stretching mode of the HPO_4^{2-} group. For increasing value of FS in the coating composite, the peak intensity decreases due to the decreased amount of HA. This confirms that the coating has FS too. Although the synthesized FS is very weakly Raman active, as shown by the Raman spectrum of pure FS coating with a very small peak at 858 cm^{-1}, it can be deduced that the coating has both HA and FS. Further, no Raman peak appears either at 556 cm^{-1} or at 716 cm^{-1}, giving the idea that the coating is uniform and corrosion effect is absent from the surface of the stainless steel, making it more suitable for biomedical applications.

Conclusions. The background and noise in the Raman spectrum are some of the main reasons preventing the application of such a powerful tool in material analysis. The efficient removal of background can lead to an easy and accurate analysis of materials using Raman spectroscopy. This work successfully evaluated the efficiency of some background and noise removal techniques to the Raman spectrum. The results from the spline fitting method show that it can maintain the significant peaks in the spectrum, while efficient background removal from all of the four types of background generally arises in the Raman signal. Subsequent denoising using the wavelet method keeps the Raman intensity almost near to the original background removed signal while increasing SNR with a high value of goodness of fit. From the above discussion, we can conclude that spline fit background removal followed by wavelet denoising can work efficiently for Ra-

man signal. We also successfully analyzed the HA-FS coated stainless steel Raman spectrum for the composition of the thin film. From pure HA to composite of HA-FS to pure FS, there is a large variation in the Raman peak, which confirms the composition of the coating. In the future, there is a need for detailed structural analysis of coatings, which may be done with Raman spectroscopy for better characterization.

Acknowledgments. This work is supported by the Centre for Interdisciplinary Research (CIR) and Technical Education Quality Improvement Programme, Phase-II (TEQIP-II) and Phase-III (TEQIP-III), Motilal Nehru National Institute of Technology Allahabad, Prayagraj, UP, India. The authors give special thanks to Dr. Animesh Ojha and Dr. Naresh Kumar from the Department of Physics, MNNIT Allahabad, Prayagraj, India, for his valuable contribution to the successful conduction of the experiments and characterizations.

Declaration of conflicting interests. The author(s) declared no potential conflicts of interest concerning the research, authorship, and/or publication of this article.

REFERENCES

1. S.-I. Akimoto, Y. Matsui, Y. Syono, *The Physics and Chemistry of Minerals and Rocks*, 327 (1976).
2. S. Ramesh, A. Yaghoubi, K. S. Lee, K. C. Chin, J. Purbolaksono, M. Hamdi, M. A. Hassan, *J. Mech. Behav. Biomed. Mater*., **25**, 63 (2013).
3. S. Ni, L. Chou, J. Chang, *Ceram. Int*., **33**, 83 (2007).
4. S. R. Levitt, P. H. Crayton, E. A. Monroe, R. A. Condrate, *J. Biomed. Mater. Res*., **3**, 683 (1969).
5. M. H. Fathi, A. Hanifi, *Mater. Lett*., **61**, 3978 (2007).
6. Y.-M. Sung, J.-C. Lee, J.-W. Yang, *J. Cryst. Growth*, **262**, 467 (2004).
7. Y.-M. Sung, D.-H. Kim, *J. Cryst. Growth*, **254**, 411 (2003).
8. M. A. Minnath, In *Fundamental Biomaterials: Metals*, Elsevier, 167–174 (2018).
9. I. Milošev, *Pure Appl. Chem*., **83**, 309 (2010).
10. M. A. Ward, T. K. Georgiou, *Polymers*, **3**, 1215 (2011).
11. I. Ibrahim, E. Sadiku, T. Jamiru, A. Hamam, W. K. Kupolati, *Curr. Trends Biomed. Eng. Biosci.*, **4**, 9 (2017).
12. J. Chevalier, L. Gremillard, *J. Eur. Ceram. Soc*., **29**, 1245 (2009).
13. A. Iftekhar, *Standard Handbook of Biomedical Engineering and Design*, McGraw-Hill Companies (2004).
14. L. Zhao, P. K. Chu, Y. Zhang, Z. Wu, *J. Biomed. Mater. Res., Part B: Appl. Biomater.*, **91**, 470 (2009).
15. L. A. Thomson, F. C. Law, N. Rushton, J. Franks, *Biomaterials*, **12**, 37 (1991).
16. L. Tang, P. Thevenot, W. Hu, *Curr. Top. Med. Chem.*, **8**, 270 (2008).
17. K. De Groot, J. G. C. Wolke, J. A. Jansen, *Proc. Inst. Mech. Eng., H: J. Eng. Med.*, **212**, 137 (1998).
18. J. A. Davidson, P. Kovacs, US Patent 5, **169**, 597 (December 1992).
19. P. S. Prakash, S. J. Pawar, R. P. Tewari, *Proc. Inst. Mech. Eng., L: J. Mater.: Des. Appl.,* 1464420717705151 (2017).
20. H. Khandelwal, G. Singh, K. Agrawal, S. Prakash, R. D. Agarwal, *Appl. Surf. Sci.*, **265**, 30 (2013).
21. T. J. Vickers, R. E. Wambles Jr., C. K. Mann, *Appl. Spectrosc*., **55**, 389 (2001).
22. http://www.Chem.Uoa.Gr/Applets/Appletsmooth/Appl_smooth2. Html (Background on Ensemble Averaging) (2013).
23. A. Savitzky, M. J. Golay, *Anal. Chem*., **36**, 1627 (1964).
24. F. Ehrentreich, L. Sümmchen, *Anal. Chem*., **73**, 4364 (2001).
25. H. Chen, W. Xu, N. Broderick, J. Han, *J. Raman Spectrosc*., **49**, 1529 (2018).
26. K. F. McCarty, D. R. Boehme, *J. Solid. State Chem*., **79**, 19 (1989).
27. J. E. Maslar, W. S. Hurst, W. J. Bowers Jr, J. H. Hendricks, *Corrosion*, **58**, 739 (2002).
28. B. Mihailova, B. Kolev, C. Balarew, E. Dyulgerova, L. Konstantinov, *J. Mater. Sci*., **36**, 4291 (2001).
29. D. C. O'shea, M. L. Bartlett, R. A. Young, *Arch. Oral Biol*., **19**, 995 (1974).
30. W. P. Griffith, *J. Chem. Soc. A: Inorg., Phys., Theor.*, 286 (1970).
31. G. R. Sauer, W. B. Zunic, J. R. Durig, R. E. Wuthier, *Calcified Tissue Int*., **54**, 414 (1994).
32. B. O. Fowler, M. Markovic, W. E. Brown, *Chem. Mater*., **5**, 1417 (1993).
33. H. Tsuda, J. Arends, *J. Dent. Res*., **72**, 1609 (1993).